Journal of Magnetic Resonance **156,** 26–40 (2002)
doi:10.1006/jmre.2002.2531

Universal Equations for Linear Adiabatic Pulses and Characterization of Partial Adiabaticity

Yasvir A. Tesiram and M. Robin Bendall[1]

The Russell Grimwade School of Biochemistry and Molecular Biology, University of Melbourne, Parkville 3052, Victoria, Australia

Received August 29, 2001; revised December 21, 2001; published online May 31, 2002

A numerical analysis of the sech/tanh (or hyperbolic secant) and tanh/tan adiabatic inversion pulses provides a set of master equations for each type of pulse that guarantee their optimal implementation over a wide range of practical conditions without needing to further simulate the inversion profiles of the pulses. These simple equations determine the necessary maximum RF amplitude (RF_{max}) required for a preselected degree of inversion across a chosen effective bandwidth (bw_{eff}) and for a chosen pulse length (T_p). The two types of pulse function differently: The sech/tanh pulse provides a rectangular inversion profile with bw_{eff} being a large fraction of the adiabatic frequency sweep (*bwdth*), whereas for tanh/tan bw_{eff} is $\leq bwdth/20$. If the quality of inversion is defined as the minimum allowable extent of inversion, ι_{bw}, at the boundaries of bw_{eff}, two basic linear equations are found for both types of pulse and these are of the form $(RF_{max}T_p)^2 = m_1\, T_p bwdth + c_1$ and $T_p bwdth = m_3 T_p\, bw_{eff} + c_3$. The different behavior of the two pulses is expressed as different dependencies of the slopes m_n and intercepts c_n on ι_{bw} and allowances are made for second order effects within these equations. The availability of these master relationships enables a direct comparison of the two types of adiabatic pulse and it is found that tanh/tan requires about half the pulse length of an equivalent sech/tanh pulse and also has the advantage of being less sensitive to the effects of scalar coupling. In contrast sech/tanh delivers about half the total RF power of an equivalent tanh/tan pulse. It is expected that the forms of these two basic linear equations are generally applicable to adiabatic inversion pulses and thus define the concept of "linear adiabaticity." At low values of $T_p bwdth$ or $T_p\, bw_{eff}$ the linear equations no longer apply, defining a region of "partial adiabaticity." Normal adiabatic pulses in the middle of this partial region are more efficient in terms of RF_{max} or T_p but are moderately less tolerant to RF inhomogeneity. A class of numerically optimized pulses has recently been developed that specifically trades adiabaticity in an attempt to gain RF_{max} or T_p efficiency. In comparison to normal adiabatic pulses implemented under optimal conditions, these new partially adiabatic pulses show only marginal improvements; they are restricted to single values of $T_p\, bw_{eff}$, and they are vastly less tolerant to RF inhomogeneity. These comparisons, and direct comparisons between any types of inversion pulse, adiabatic or otherwise, can be made using plots of $(RF_{max}\, T_p)^2$ or (Total Power) T_p versus $T_p\, bw_{eff}$.

Key Words: **adiabatic pulses; sech/tanh; tanh/tan; master equations; partial and linear adiabaticity.**

INTRODUCTION

Adiabatic inversion pulses will play an important role in high-resolution NMR spectroscopy particularly for the automation of pulse sequence methods (*1*) and for greater bandwidths as larger magnetic fields become available. Their unique and valuable property is their consistent 180° spin rotations independent of any variation in RF amplitude above a minimum limiting value. We provide universally applicable master equations that relate the five experimental variables of prime importance and so determine the most efficient general conditions for the implementation of these pulses. This analysis was undertaken for two types of adiabatic inversion pulse widely used in MRI and MRS: The hyperbolic secant or sech/tanh (amplitude/frequency modulation) pulse (*2*) and the tanh/tan pulse (*3, 4*).

One criticism of adiabatic pulses has been that they are too long for applications in high resolution NMR. However, it has been shown experimentally (*5*) and proven rigorously (*6*) that scalar coupling proceeds normally during such pulses, but with reduced effective coupling constants. This reduction is only $\approx$10% and adiabatic pulses can occupy the whole of $(2J)^{-1}$ delay periods in pulse sequences and thus increase these delays by only 10%. For example, 3-ms sech/tanh pulses can be used in ^{1}H–^{13}C NMR and bandwidths up to about 500 kHz with standard RF amplifiers and NMR probes can be obtained, vastly more than is normally required.

Nevertheless, if available peak RF amplitude (RF_{max}) is insufficient for a sech/tanh inversion pulse, adiabatic pulses with lower constant or near constant RF amplitude can still be employed. During the last 20 years this type of adiabatic pulse has evolved and improved from the first crude example, a constant/linear or CHIRP pulse (*7*), to the constant/tan variation (*8*) and the tanh/tan pulse (*3, 4*). In the latter the RF amplitude is smoothly but rapidly increased to a maximum value so that it is constant across about 90% of the pulse, so eliminating Gibbs overshoot "wobbles" arising from the extreme boundary truncation of a rectangular RF function.

[1] To whom correspondence should be addressed at Adiabatics Inc., 83 S. Branciforte Ave., Santa Cruz, CA 95062. E-mail: robin@gonmr.com.

1090-7807/02 $35.00

Composite inversion pulses can also be designed to cover large bandwidths but they have not been shown to be competitive with adiabatic pulses in terms of maximum bandwidth, minimum power deposition, and ability to change the bandwidth using the same pulse. As demonstrated emphatically by the development of adiabatic decoupling (e.g., (*9, 10*)), the bandwidth of an adiabatic pulse increases in proportion to RF^2_{max}, whereas that of a composite pulse increases only linearly with RF amplitude.

Numerical optimization strategies have been used to design adiabatic pulses for specific purposes (e.g., (*11–13*)) and are consequently not as generally applicable as pulses with analytic waveforms such as sech/tanh or tanh/tan. Furthermore the digital lists for the waveforms of numerically optimized pulses must be calculated in advance of experiment whereas analytic waveforms are generated from mathematical functions that are easily implemented "on the fly" with computer macros. In later sections we compare the sech/tanh and tanh/tan pulses with a new class of numerically optimized pulse designed to take advantage of partial adiabaticity. This comparison helps justify the need to determine the optimum conditions for analytic adiabatic pulses as accomplished in this paper.

BACKGROUND AND METHODS

In keeping with our previous nomenclature (*5, 9, 10*), the sech/tanh amplitude and frequency modulations are

$$B_1 = RF_{max}\,\mathrm{sech}\,\beta(1 - 2t/T_p); \quad [1]$$

$$\Delta H = (bwdth/2)[\tanh\beta(1 - 2t/T_p) + s], \quad [2]$$

where the amplitude truncation is determined by $\mathrm{sech}\,\beta = 0.01$ ($\beta = 5.3$); T_p is the pulse length; the bandwidth of the frequency sweep is $\pm bwdth/2$; and s is the dimensionless resonance offset of the pulse in units of $bwdth/2$ where $s = 0$ denotes an on-resonance pulse. The corresponding equations for the first half of the tanh/tan pulse are

$$B_1 = RF_{max}\,\tanh\zeta t/T_p; \quad [3]$$

$$\Delta H = (bwdth/2)[\tan\kappa(1 - 2t/T_p) + s]/\tan\kappa, \quad [4]$$

where $\zeta = \tan\kappa = \tan 0.968\pi = 20$, and the second-half equations are the time-reversed equivalents of Eqs. [3] and [4] (*3, 4*). Throughout, RF_{max} and $bwdth$ are in units of kilohertz with T_p in milliseconds. (Alternative parameterizations and units for the sech/tanh pulse can be found in Ref. (*14*) where $RF_{max} \equiv q|F|$, $\beta \equiv \lambda/2$, $bwdth \equiv 2|F|$, and $T_p = T$.)

The adiabatic condition requires the quantity $|d\alpha/dt|/B_e$ to be small, where α is the angle the effective RF field B_e makes with the xy plane of the rotating reference frame, given by $\tan\alpha = \Delta H/B_1$. Defining the usual scaling factor, $v = RF_{max}/(bwdth/2)$, for any adiabatic pulse

$$|d\alpha/dt|/B_e = bwdth/\left[RF^2_{max}T_p f_1(v, s, t)\right] = [T_p bwdth\, f_2(v, s, t)]^{-1}, \quad [5]$$

where f_1 and f_2 depend on the forms of the amplitude/frequency functions of the pulse. For adiabatic decoupling ((*9, 10*) and references cited therein), we found that at constant T_p, decoupling efficiency had a common dependence on $bwdth/RF^2_{max}$ and this derived from a common dependence of inversion efficiency at the center of the bandwidth for single inversion pulses on $bwdth/(RF^2_{max}T_p)$ since from Eq. [5] this factor ensures some commonality in adiabaticity. Furthermore, we found linear relations between $bwdth$ and effective bandwidth, bw_{eff}, for both single pulses and decoupling and in the case of single pulses at constant T_p the relationship was particularly simple and given by

$$bwdth = c + bw_{eff}. \quad [6]$$

In other work (*5*) we noted a commonality of attributes for the sech/tanh pulse at constant $T_p bwdth$, which is also attributable to the adiabatic condition as in Eq. [5]. This dimensionless quantity, $T_p bwdth$, is familiar as the R value or factor in many references describing adiabatic pulses (e.g., (*1, 3, 4, 11*)) but here we will continue to write it explicitly to more easily keep in mind its meaning. In preliminary calculations for this article we found a linear relation between the reciprocals of $bwdth/(RF^2_{max}T_p)$ and $T_p bwdth$ for the sech/tanh pulse, which can be recast more conveniently as a linear relation between $(RF_{max}T_p)^2$ and $T_p bwdth$ and this forms the basis of our master equations determined below.

It is possible to derive algebraic equations for the evolution of the effective field B_e during an adiabatic pulse and in some studies (e.g., (*5, 15*)) this has provided valuable basic theory. But this method is only relevant if the spins closely follow B_e throughout the pulse; i.e., the pulse is nearly 100% adiabatic. Here we are concerned with finding equations for optimal conditions at variable extents of inversion across the entire effective bandwidth. Clearly the spins do not always closely follow B_e under such circumstances. Consequently, our approach has been to numerically simulate adiabatic pulses over a wide range of conditions to determine the relevant master equations.

For this study we designate the amount of $-z$ magnetization after the pulse at the center of the inversion profile as the inversion number, ι_o, so that

$$\text{percent inversion} = 50(1 + \iota_o). \quad [7]$$

For experimental applications the user needs to know the appropriate values of RF_{max}, T_p, and $bwdth$ for a chosen effective bandwidth, bw_{eff}, and a chosen amount of inversion guaranteed across bw_{eff}. Thus the degree to which the inversion number is

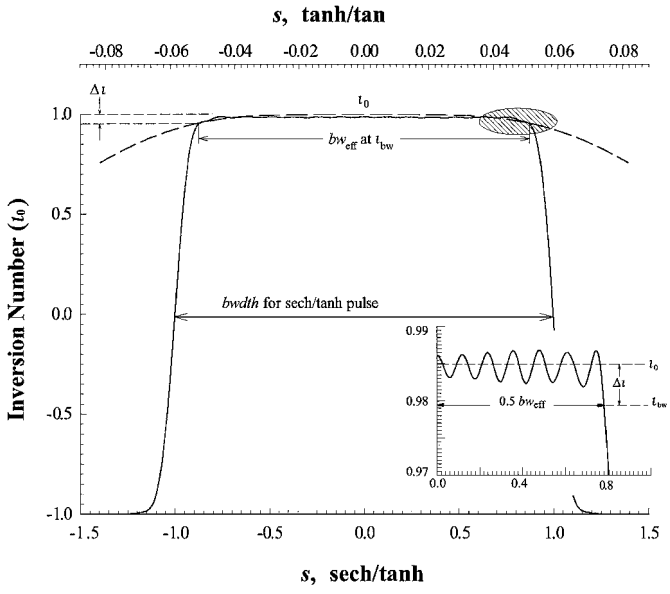

FIG. 1. A typical inversion profile for the sech/tanh pulse (solid line; T_p = 1.0 ms, $bwdth = 32$ kHz, $RF_{max} = 8.78$ kHz, $bw_{eff} = 25.0$ kHz, $\iota_o = 0.985$, and $\Delta\iota = 0.005$) matched with a comparable tanh/tan pulse (dashed line; T_p = 1.0 ms, $bwdth = 612$ kHz, $RF_{max} = 6.13$ kHz, $bw_{eff} = 25.0$ kHz, $\iota_o = 0.996$, and $\Delta\iota = 0.016$). The user must choose a minimum inversion number, ι_{bw}, defining the effective bandwidth bw_{eff} and thus an acceptable quality for inversion across the spectral width. The effective bandwidths for the two types of inversion profile are indicated in units of $bwdth/2$ showing that the tanh/tan pulse acts to uniformly invert only a small fraction of the $bwdth$ value. The inversion number on resonance, ι_o, which determines RF_{max}, should be greater by an amount $\Delta\iota$ than ι_{bw}, the number defining bw_{eff}. For the sech/tanh pulse, $\Delta\iota$ should be sufficient so that the profile "wobbles" in the shoulder region (shaded) lie above the ι_{bw} value defining bw_{eff}. This is illustrated further in the figure inset, an expanded view of the shoulder region. From the calculations leading to Fig. 5, the minimum practical $\Delta\iota$ was found to be 0.005 units for the sech/tanh pulse.

allowed to deteriorate, $\Delta\iota = \iota_o - \iota_{bw}$, at the extremes of bw_{eff}, must also be selected, as illustrated in Fig. 1 for typical simulations of frequency profiles.

Numerical simulations were made using Pulsetool, a Varian computer program for Bloch equation calculations that applies a 3×3 rotation matrix for each digitized time increment in a modulated RF pulse, and 1000 points across the frequency axis were calculated for every profile. Phase increments that correspond to the integral of the frequency sweep functions, Eqs. [2] and [4], were employed. T_p was varied in the ranges of 0.25–3 ms and 0.025–2 ms, and $bwdth$ was varied in the ranges of 5–120 kHz and 75–5000 kHz for sech/tanh and tanh/tan, respectively.

RF_{max} values were measured at chosen inversion numbers ι_o in the range 0.8–0.996 for sech/tanh and at $\iota_o = 0.996$ for tanh/tan for many combinations of T_p and $bwdth$. Complete inversion profiles at these calibrated RF_{max} values were simulated to determine bw_{eff} at different inversion numbers ι_{bw} in the range 0.6–0.996 for sech/tanh and 0.9–0.996 for tanh/tan. Second-order modulations or "wobbles" across the sech/tanh inversion profile, which are most severe at the shoulders of the inversion profile as indicated in the inset to Fig. 1, complicated these measurements to the extent of creating scatter in the data points from the various linear relationships found. For example, a wobble can add to the profile shoulder and increase bw_{eff} or subtract from the shoulder and decrease bw_{eff}. Values of bw_{eff} at $\iota_{bw} = \iota_o$ were obtained by ignoring the negative excursions of the wobbles below ι_{bw} with the limit of the effective bandwidth determined by the excursion of the shoulder below ι_{bw}. The minimum $\Delta\iota$ to prevent these negative excursions was found to be 0.005 units for $T_p bwdth \leq 100$ increasing to 0.01 units at $T_p bwdth = 300$. The tanh/tan pulse never yields a flat profile so bw_{eff} must always be measured at an inversion number ι_{bw} less than ι_o.

Inversion profiles were initially digitized in 1000 steps, but during the course of the study it was found that $T_p bw_{eff}$ values above 70 increasingly generate high frequency oscillations across the profiles of both types of pulse. Accordingly, the minimum number of waveform increments was set at $1000 T_p bw_{eff}/70$. This problem presumably arises because the number of steps in the digitized phase waveform is insufficient to correspond to a smooth frequency sweep. Nevertheless, the phenomenon cannot be explained in terms of a required minimum phase increment since the minimum increment for tanh/tan is about a factor 20 larger than that of the sech/tanh pulse.

THE SECH/TANH (HYPERBOLIC SECANT) PULSE

Numerical Analysis

Excellent linear plots of $(RF_{max} T_p)^2$ versus $T_p bwdth$ were obtained for selected on-resonance efficiencies for the sech/tanh pulse as shown in Fig. 2. However, from the inset to Fig. 2 and as expected from prior work (*5*), there is an increasing divergence of the data from the fitted straight lines for $T_p bwdth$ values less than 10 resulting from an increasing violation of the adiabatic limit.

The slopes, m_{RF}, and intercepts, c_{RF}, of these linear plots, which are given by

$$(RF_{max} T_p)^2 = m_{RF} T_p bwdth + c_{RF}, \qquad [8]$$

are replotted in Fig. 3 as $1/m_{RF}^2$ and $1/c_{RF}$ against inversion number ι_o, yielding

$$1/m_{RF}^2 = -2.695\iota_o + 2.809 - 1.5 \times 10^{-4}/(1 - \iota_o); \qquad [9]$$

$$1/c_{RF} = +2.885\iota_o - 2.999 + 1.4 \times 10^{-4}/(1 - \iota_o). \qquad [10]$$

The first two terms in Eqs. [9] and [10] correspond to the straight line fits to the data for $\iota_o \leq 0.98$ (shown in Fig. 3), which are sufficiently accurate to calibrate pulses for most practical experimental conditions. For ι_o values very close to one, RF_{max} tends to infinity so that m_{RF} goes to zero, and to fit the data

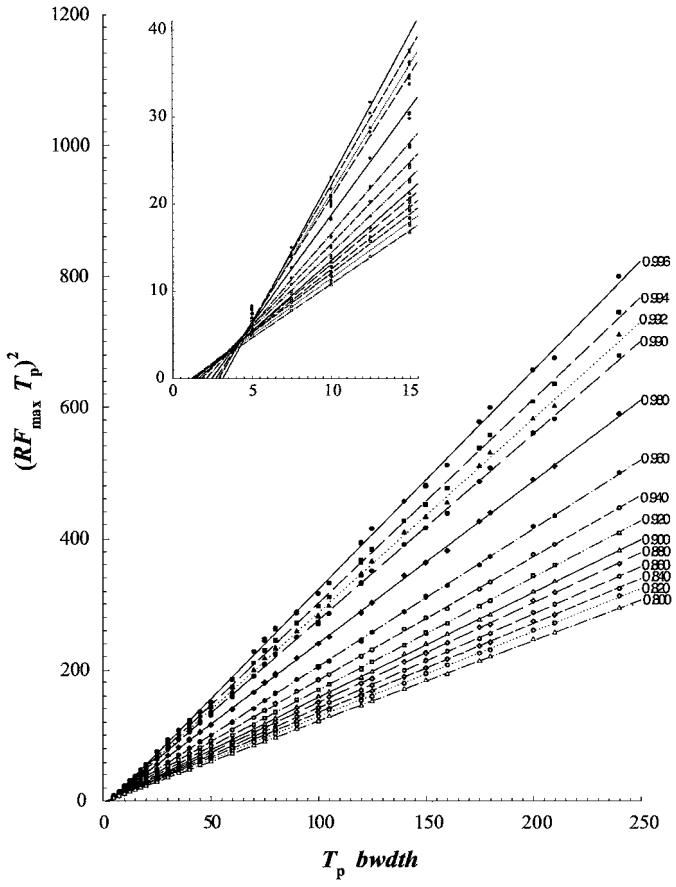

FIG. 2. Plots of $(RF_{\max}T_{\rm p})^2$ versus $T_{\rm p}bwdth$ for the sech/tanh pulse at various inversion numbers on resonance $\iota_{\rm o}$ from 0.996 to 0.800. These plots are fitted to straight lines, given by Eq. [8] with correlation coefficients (r^2) greater than 0.999. The data set comprises 55 simulated pulses at each inversion level including duplicate measurements for $T_{\rm p}bwdth = 5, 10, 20, 30, 60, 90, 120, 100$, and 150 arising from different combinations of *bwdth* and $T_{\rm p}$. The inset provides an expanded view for low $T_{\rm p}bwdth$ values showing increased deviation from the regression lines for $T_{\rm p}bwdth$ values less than 10.

the third hyperbolic correction term is required. The complete equations [9] and [10] should be employed for high values of $\iota_{\rm o}$, for example, to avoid 0.5% losses in S/N when using numerous sech/tanh pulses in an NMR pulse sequence.

As depicted in Fig. 1, the effective bandwidth $bw_{\rm eff}$ is always less than *bwdth* because the frequency profile for a sech/tanh pulse is not perfectly rectangular and *bwdth* reflects the width of the profile at half height, i.e., at $s = \pm 1$. Plots of the dimensionless quantities $T_{\rm p}bw_{\rm eff}$ versus $T_{\rm p}bwdth$ were made as illustrated in Fig. 4. These plots were always linear and had slopes within 1% of unity. Thus, the extensive data obtained fit the simple equation

$$T_{\rm p}bw_{\rm eff} = T_{\rm p}bwdth - c_{\rm bw}, \qquad [11]$$

in agreement with Eq. [6]. The overall shape of the inversion profile does not change greatly with $\iota_{\rm o}$ so that $c_{\rm bw}$ is independent of $\iota_{\rm o}$ as exemplified by a comparison of the data for $\iota_{\rm o} = 0.98$ and 0.88 in Fig. 4. Instead, $c_{\rm bw}$ depends on $\Delta\iota$, where $\Delta\iota = \iota_{\rm o} - \iota_{\rm bw}$, and a plot of $c_{\rm bw}$ versus $\Delta\iota$ can be fitted to an equation of the form $y = (ax + b)^{-0.5} + 1$. Transposing this yields a linear plot of $(c_{\rm bw} - 1)^{-2}$ versus $\Delta\iota$ as in Fig. 5. The scatter of data points in Fig. 5 arises chiefly from wobbles on the profile shoulder (illustrated in the inset to Fig. 1) which can increase or decrease the effective bandwidth. These deviations are less for larger $\Delta\iota$ since this increasingly avoids the shoulder region. For reliable experimental implementation of a master equation, a user will normally prefer a guaranteed effective bandwidth rather than one which might turn out to be a few percent too small. Accordingly two further straight lines are provided in Fig. 5 corresponding to a minimal limit on $(c_{\rm bw} - 1)^{-2}$ and thus an upper bound on $c_{\rm bw}$. Transposing the formulae for these straight lines via the appropriate positive roots yields

$$c_{\rm bw} = (2.44\Delta\iota - 0.003)^{-0.5} + 1, \qquad \Delta\iota \geq 0.02; \quad [12]$$

$$c_{\rm bw} = (0.85\Delta\iota + 0.025)^{-0.5} + 1, \qquad \Delta\iota < 0.02. \quad [13]$$

Use of these equations ensures that $bw_{\rm eff}$ is not underestimated.

Practical Implementation of sech/tanh Pulses for the Broadband Inversion of Spins

For experimental application of sech/tanh pulses over a wide range of conditions, the universal master expression [8] should be used. Subsidiary Eqs. [9]–[13] provide the values of $m_{\rm RF}$, $c_{\rm RF}$,

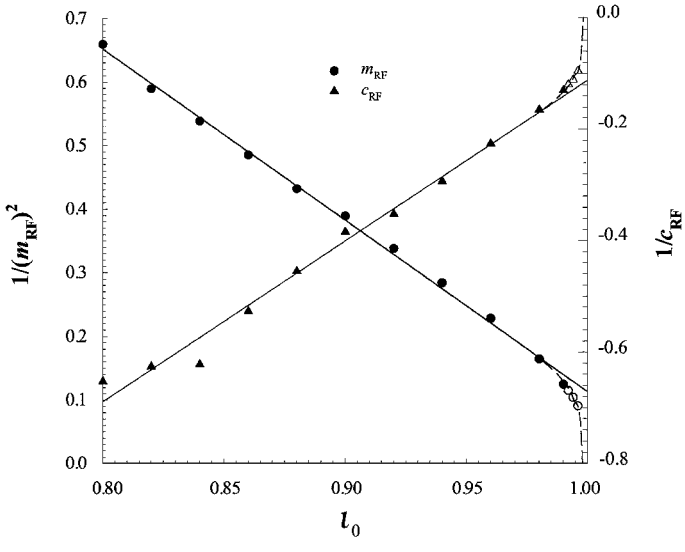

FIG. 3. Linear plots of the inverse square of the slope $m_{\rm RF}$ and the inverse of the intercept $c_{\rm RF}$, from Fig. 2, versus inversion number $\iota_{\rm o}$ ($r^2 = 0.997$ and 0.988, respectively). Data points for $\iota_{\rm o} \geq 0.99$ have been omitted from the linear regression calculations. The dashed curves ($r^2 = 0.999$ and 0.992, respectively) given by Eqs. [9] and [10], which are indistinguishable from the straight lines for $\iota_{\rm o} \leq 0.98$, correspond to the addition of hyperbolic correction terms to the initial linear equations.

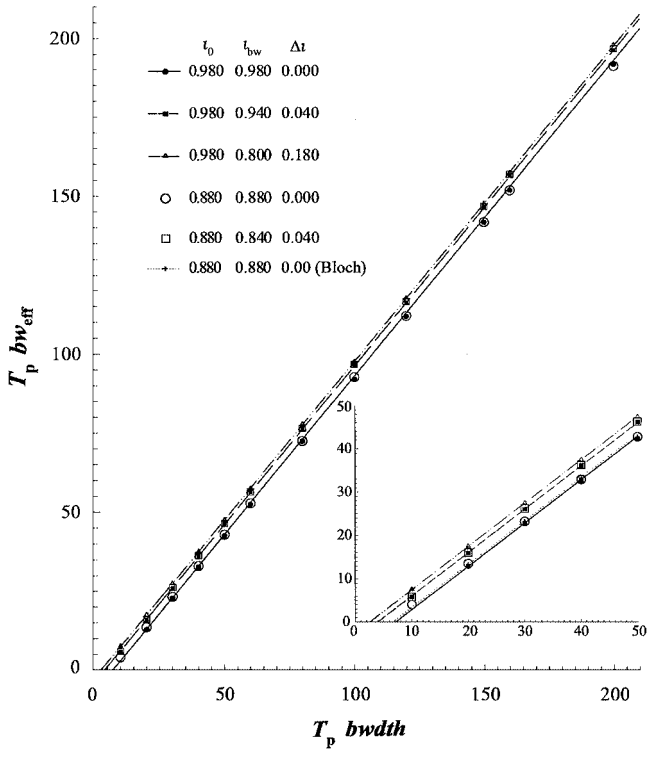

FIG. 4. Examples of plots of $T_p bw_{eff}$ versus $T_p bwdth$ for the sech/tanh pulse for on-resonance inversion number $\iota_o = 0.98$ at $\Delta\iota = 0$, 0.04 and 0.18 fitted to straight lines. Inversion profiles used for the measurement of bw_{eff} were generated for chosen $bwdth$ and T_p and values of RF_{max} were calculated according to Eq. [8]. The slopes of the regression lines fitted to these and similar data, comprising 16 such lines for $\Delta\iota$ ranging from 0 to 0.18, averaged 0.998 and were within a range of less than 1% of unity (intercepts ranged from −7.2 to −2.5). Consequently the straight line fits shown in this figure and used in Fig. 5 assume a unit slope. Superimposed in large open symbols are data for $\iota_o = 0.88$, and $\Delta\iota = 0$ and 0.04, indicating excellent correspondence between regression lines calculated for different ι_o at constant $\Delta\iota$, particularly at larger $T_p bwdth$ and $\Delta\iota$. The additional dotted regression line in the expanded inset plot has been derived from inversion profiles generated with exact values of RF_{max} at $\iota_o = 0.88$ calculated from the Bloch equation, and it differs only slightly from the corresponding line for RF_{max} obtained from Eq. [8].

c_{bw}, and $bwdth$ after selection of appropriate values of ι_o and $\Delta\iota$. Having first chosen an acceptable value of ι_{bw}, the required effective bandwidth bw_{eff}, and a reasonable value for T_p, Eq. [11] provides the value of $bwdth$ and master Eq. [8] determines the necessary minimum value for RF_{max}. As a quick alternative, RF_{max} can be estimated from the contour plot in Fig. 6, which guarantees 99% inversion ($\iota_{bw} = 0.98$) across the effective bandwidth and Eqs. [13] and [11] yield $bwdth = bw_{eff} + 6.85/T_p$. For example, the ^{13}C shift range of 200 ppm at 600 MHz (30 kHz) can be inverted with a 0.4 ms sech/tanh pulse given an available RF field of 17 kHz (a typical 15-μs ^{13}C 90° pulse time). Since all adiabatic pulses function better with more RF power, the user may add a further 5–10% to the minimum RF amplitude (or equivalently increase T_p by 10–20%) as insurance against miscalibrations, RF inhomogeneity, or hardware variation.

A scrutiny of the wobbles in the shoulder region, illustrated in the inset to Fig. 1, determined that a minimum $\Delta\iota = 0.005$ should be used to ensure that ι_{bw} lies below these wobbles. Equation [8] is thus applicable to the range, $0.7 \le \iota_{bw} \le 0.99$, or a usual working range of 85–99.5% inversion of the nuclear spins. From Fig. 2, this master equation should also be applicable to the range $10 \le T_p bwdth \le 250$.

The equations were checked for accuracy by selecting ι_o, $\Delta\iota$, bw_{eff}, and T_p, calculating $bwdth$ and RF_{max}, simulating the pulse profile, and measuring the actual ι_o and bw_{eff} obtained. A total of 85 checks were made over the ranges $\iota_o = 0.85$–0.995, $\Delta\iota = 0.005$–0.1, $T_p = 0.05$–60 ms, and $bw_{eff} = 5$–200 kHz, yielding the ranges $T_p bwdth = 13$–300 and $RF_{max} = 0.3$–125 kHz. The extent of inversion ι_o at zero frequency offset was predicted with extreme accuracy, the average error being only $+0.05 \pm 0.07\%$ of inversion efficiency. The error in predicting effective bandwidths was an average of $+0.27 \pm 0.95\%$ over most of the $T_p bwdth$ range increasing to $+3.7 \pm 1.4\%$ for $T_p bwdth < 20$ where poorer agreement was expected. The goal of attempting to slightly overestimate ι_o and bw_{eff} was thus largely achieved. The largest negative errors were underestimates of -0.8% of bw_{eff} for $\Delta\iota < 0.02$ concurrent with $T_p bwdth \ge 100$ caused by an increasingly complex pattern of wobbles on the profile shoulder with increasing $T_p bwdth$. Even these small unwanted deviations could be eliminated by introducing a slope $m_{bw} = 1.008$ (i.e., a 0.8% increase) into Eq. [11]. This was simple to implement (for the ranges $\Delta\iota < 0.02$ and $T_p bwdth > 100$) in a

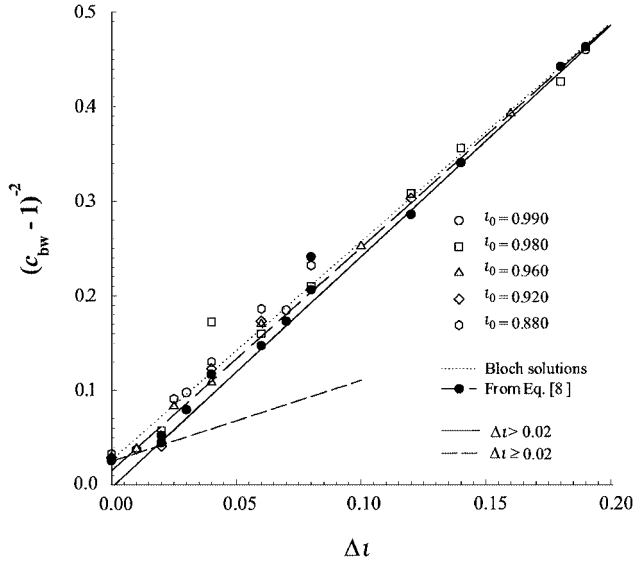

FIG. 5. The intercepts from Fig. 4 plotted as $1/(c_{bw} - 1)^2$ versus $\Delta\iota$ fitted to straight lines ($r^2 \ge 0.991$). Open data points (dotted line) are from a data set created by Bloch equation simulations and the solid data points (dashed line) are from a data set where RF_{max} was calculated according to Eq. [8] for $\iota_o = 0.980$. The positive root of $(c_{bw} - 1)^2$ should be taken to determine c_{bw}. Minimum acceptable values of c_{bw} for experimental applications are given by the two additional straight lines, $(c_{bw} - 1)^{-2} = 2.44\Delta\iota - 0.003$ and $(c_{bw} - 1)^{-2} = 0.85\Delta\iota + 0.025$, corresponding to $\Delta\iota \ge$ or <0.02, respectively.

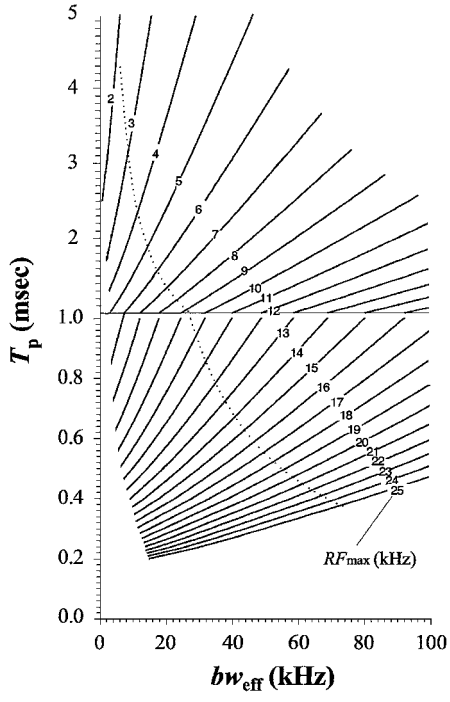

FIG. 6. Contour plots of RF_{max} required for a sech/tanh inversion pulse, calculated from master Eq. [8], to guarantee 99% inversion across the chosen effective bandwidth at selected values of pulse length T_p ($\iota_o = 0.985$; $\Delta\iota = 0.005$; $\iota_{bw} = 0.98$). The boundary in the bottom left corner corresponds to an adiabatic limit of $T_p bwdth = 10$ ($T_p bw_{eff} = 3$ for $\Delta\iota = 0.005$). The boundary in the top right corner is determined by $T_p bwdth = 300$, the extent of our numerical checks of Eq. [8] and subsidiary equations. The dotted line through the middle of the contours corresponds to $v = 2RF_{max}/bwdth = 0.5$ with $bw_{eff} = 0.8\,bwdth$ and T_p from Eq. [11].

short software macro written to automatically quantify *bwdth* and RF_{max} and this modification changes the error in predicting effective bandwidths to $+0.61 \pm 0.71\%$.

A common use of adiabatic inversion pulses will be at the center of $(2J)^{-1}$ modulation periods in heteronuclear pulse sequences. The effect of reduced scalar coupling can be determined from Fig. 10 of Ref. (*5*), or from the analytical equations in Ref. (*15*) which provide the ratio of the reduced coupling to the normal coupling constant, J_r/J_o, as a function of the dimensionless quantities $v(= 2\,RF_{max}/bwdth)$ and resonance offset, s. Allowance should be made for the slower J modulation effects during an adiabatic pulse by increasing the total time $(2J)^{-1}$ by an amount given by $(1 - J_r/J_o)T_p$. The dotted curved line in Fig. 6 corresponds to $v = 0.5$, a typical value, and from Fig. 10 of (*5*) the average of J_r/J_o at $s = 0$ and $s = \pm 0.8$ at $v = 0.5$ requires an increase in the total $(2J)^{-1}$ period by 12.5% of T_p. If the $(2J)^{-1}$ period is adjusted in this way there will nevertheless be a small loss in signal intensity from the variation in J_r/J_o across the bandwidth. If bw_{eff} is limited to 90% of *bwdth* there is a maximum loss of signal at $s = \pm 0.9$ of 2% for $v = 2$ decreasing to 1% for small v. These losses apply to a pulse that occupies the whole of a $(2J)^{-1}$ period and become insignificant for shorter pulses. For example, for a 1-ms pulse in a 3-ms $(2J)^{-1}$ delay the maximum signal loss is only 0.2%. The losses are smaller or zero for $|s| < 0.9$ but rapidly increase for $|s| > 0.9$. It is easy to model the curves in Fig. 10 of (*5*) with polynomials so these modest corrections can be handled routinely by software macros.

In consequence, there are three recommendations for the use of sech/tanh pulses at the center of $(2J)^{-1}$ modulation periods: Add an amount equal to $(1 - J_r/J_o)T_p$ to the $(2J)^{-1}$ time where J_r/J_o is an average value across the effective bandwidth. Keep this correction as small as possible by using close to the maximum possible RF_{max} (avoiding amplifier compression) and thus close to the smallest possible T_p. Do not permit bw_{eff} to exceed 0.9 *bwdth* so that Eq. [11] is abandoned in favor of $bw_{eff} = 0.9\,bwdth$ whenever $c_{bw}/T_p < 0.1\,bwdth$.

Additional recommendations are provided in Ref. (*5*) to efficiently deal with J modulation effects during sech/tanh pulses at the center of $1/J$ and chemical-shift-correlation delays. Sech/tanh pulses have been used routinely as broadband inversion pulses and as semiselective pulses (discussed below) for more than 3 years in Varian's ProteinPack, a semiautomated software package of pulse sequences for protein NMR.

Selective and Semiselective sech/tanh Pulses

The rectangular shape of the inversion profile of typical sech/tanh pulses, illustrated in Fig. 1, makes them suitable for use as selective pulses. The bandwidth of the rectangular profile may be chosen to select just one segment of a spectrum, or just one edge of the profile may be positioned between spectral regions. In either case, the *bwdth* parameter defining the pulse, and used for the calibration of RF_{max} via Eq. [8], should begin and/or end midway between the selected region and the nonselected region, in contrast to broadband pulses for which the important parameter is bw_{eff}. Equation [11] characterizes the steepness of the edges of the rectangular profile and thus the discrimination between selected and nonselected spins. Accordingly, the spectral width between selected and nonselected spins, i.e., the selectivity parameter Δbw, is given by a rearrangement of Eq. [11] as

$$\Delta bw = bwdth - bw_{eff} = c_{bw}/T_p, \qquad [14]$$

which complies with an expected inverse relationship between pulse length T_p and selectivity.

Minimizing RF_{max} will not normally be an important factor, so RF_{max} can be calibrated at or above the level necessary to achieve $\iota_o = 0.996$. Setting $\Delta\iota = 0.016$ ($\iota_{bw} = 0.98$) provides the conditions necessary to ensure $\geq$99% inversion of selected spins and $\leq$1% inversion of nonselected spins, or a 100 : 1 discrimination, and Eqs. [13] and [14] yield $\Delta bw = 6.1/T_p$. If this is too ambitious, choosing $\Delta\iota = 0.092$ provides the conditions for a 20 : 1 level of discrimination and $\Delta bw = 3.1/T_p$. The product $\Delta bw T_p = 3.1$ is almost a factor of three larger than the analogous

factors for I-BURP selective 180° pulses (*16*), but *bwdth* can be changed relative to the Δbw value whereas this is a fixed ratio for the nonadiabatic I-BURP. Thus adiabatic pulses have an advantage for selecting moderate to large spectral regions, sometimes called semiselective spectroscopy. For example, if it is necessary to select a 5-kHz-wide region (as in the ^{13}C spectrum of proteins) the pulse length for an I-BURP pulse must be 1 ms and Δbw is 530 Hz for 20 : 1 discrimination. In contrast, a sech/tanh pulse delivering a 5-kHz bandwidth may still have a pulse length of 10 ms and so achieve better spectral discrimination.

THE TANH/TAN INVERSION PULSE

Numerical Analysis

The properties of tanh/tan differ strikingly from the sech/tanh pulse and so a different analytical approach is needed to determine master calibration equations. In particular, as illustrated in Fig. 1, tanh/tan does not produce a flat profile across any fraction of *bwdth* until RF_{max} is sufficiently large as to flatten the center of the inversion profile against the 100% limit ($\iota_o = 1$). If a smaller ι_o is chosen (e.g., $\iota_o = 0.996$), results follow a linear equation ($r^2 \geq 0.998$) of the same form as Eq. [8] and Fig. 2 for the sech/tanh pulse. However, the magnitude of bw_{eff} increases rapidly as a function of decreasing ι_{bw} and produces a series of straight line plots ($r^2 \geq 0.999$) of $T_p bw_{eff}$ versus $T_p bwdth$ at constant ι_{bw} given by

$$T_p bw_{eff} = m_{bw} T_p bwdth - c_{bw}, \qquad [15]$$

where the slope m_{bw} depends sensitively on ι_{bw}. This behavior contrasts with that of sech/tanh in Eq. [11] and Fig. 4.

An increase in RF_{max} above that required for $\iota_o = 0.996$ flattens the center of the inversion profile at $\iota_o = 1$ and also increases bw_{eff} and the efficiency of the pulse for chosen values of *bwdth* and ι_{bw}. To analyze this effect, it is convenient to combine the forms of Eqs. [8] and [15] to provide an initial baseline of efficiency given by

$$(RF_{max} T_p)^2 = m_{RF} T_p bw_{eff} + c_{RF}, \qquad [16]$$

and $(RF_{max} T_p)^2$ is replotted against bw_{eff} for $\Delta\iota = 0.006$ in Fig. 7a. The resulting straight line is labelled "original." Increases in RF_{max} at constant values of $T_p bwdth$ cause large increases in bw_{eff} producing parabolic curves that begin on the original straight line. A common tangent to these curves can be drawn and this straight line, labelled "optimized," represents the most efficient applications of the tanh/tan pulse, i.e., the largest bw_{eff} values for a given RF_{max}. A series of optimum tangential straight lines was also found at increasing values of $\Delta\iota$ and these are drawn in Fig. 7b. The initial choice of $\iota_o = 0.996$ is now irrelevant because a different choice would change the starting points of the parabolic curves in Fig. 7a but still yield the same parabolas and the same optimized straight line tangents. Thus the slopes m_{RF} and intercepts c_{RF} of these optimized lines depend on ι_{bw} since the link with ι_o ($\Delta\iota$ is relative to ι_o) has been eliminated. The dependence of $T_p bw_{eff}$ on $T_p bwdth$ for the optimized results, plotted in Fig. 8, demonstrates a dramatic change from the original results in that the individual lines with different

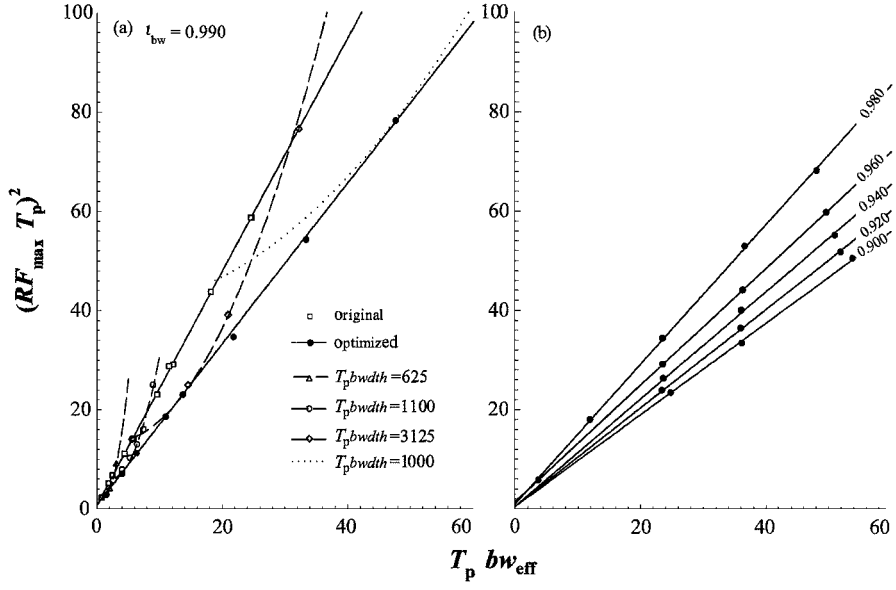

FIG. 7. (a) Plot of $(RF_{max} T_p)^2$ versus $T_p bw_{eff}$ at $\iota_{bw} = 0.990$ where RF_{max} was initially determined at various values of $T_p bwdth$ and at $\iota_o = 0.996$ by Bloch simulation. This is the "original" calibration line. Increases in RF_{max} at $T_p bwdth = 62.5$, 110, 275, 312.5, 500, 750, and 1000 (dotted curve) provided increases in $T_p bw_{eff}$ corresponding to parabolic curves, some of which are plotted, and yielded a final tangential straight line labelled "optimized." (b) Optimized lines were also determined for $\iota_{bw} < 0.990$ by finding tangents as in (a). In all cases $r^2 \geq 0.999$ for the fit of these lines to the data points corresponding to the intersection of the parabolas with a common tangent.

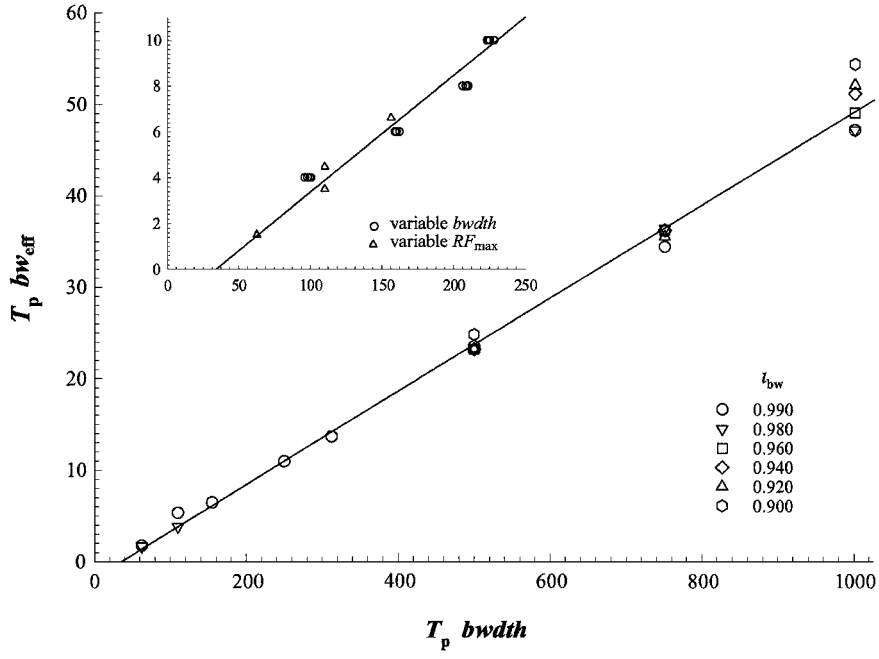

FIG. 8. Plot of $T_p bw_{eff}$ versus $T_p bwdth$ using the data points that define the optimized lines in Fig. 7 (labelled "variable RF" method in the inset). At low $T_p bwdth$ (see inset) more reliable data points were obtained by the "variable *bwdth*" method. RF_{max} was minimized at four low values of $T_p bw_{eff}$ at $\iota_{bw} = 0.99$ and 0.98 and two different values of T_p, yielding 16 additional points in the inset. The plotted straight line, corresponding to Eq. [17], is the best linear regression fit to the data in the inset that also passes through the coordinates (88,1760) or $T_p bw_{eff} = T_p bwdth/20$ at high $T_p bwdth$. The scatter of data points in the inset from the "variable RF" method of Fig. 7 reflects the difficulty of obtaining exact values from that method, whereas the scatter of the additional 16 points, which plot as four bunches, arises from a real oscillation of the best *bwdth* values about the compromise line given by Eq. [17]. This real oscillation eventually yields the expanded trajectories shown in Fig. 11 at low $T_p bw_{eff}$.

slope, given by Eq. [15], have collapsed to a single calibration line in Fig. 8. The optimized dependence is now much more similar to the behavior of sech/tanh depicted in Fig. 4.

An analysis of the results in Figs. 7 and 8 provides a basis for a master equation for the tanh/tan pulse, but it is difficult to obtain precise intercepts c_{RF} by the method illustrated in Fig. 7a, and there are second order oscillations in the data which depart from the overall linear dependencies. More accurate results were obtained by reasoning that optimal performance can be calculated by varying the *bwdth* parameter and iteratively searching for the minimum RF_{max} at fixed ι_{bw}, T_p, bw_{eff}, or equivalently, by searching for maximum bw_{eff} at fixed ι_{bw}, T_p, RF_{max}. We have since found this to be a general procedure for any adiabatic pulse and henceforth we will call this the "variable *bwdth*" method.

The large scatter of data points at $T_p bwdth = 1000$ in Fig. 8 arises from the insensitivity of bw_{eff} to varying *bwdth* at high $T_p bwdth$ since from Fig. 7a the parabola for $T_p bwdth = 1000$ intersects with the optimized tangent over a large range of $T_p bw_{eff}$ values. Application of the "variable *bwdth*" method confirms that for $T_p bwdth > 1000$, $T_p bw_{eff} = T_p bwdth/20$ is an adequate relationship, and undoubtedly the factor of 20 corresponds to tanκ in the denominator of Eq. [4]. In contrast, the estimation of bw_{eff} is sensitive to variation of *bwdth* at low values of $T_p bwdth$ and so extra data points were obtained using the more accurate "variable *bwdth*" method yielding a best straight line fit in Fig. 8 given by

$$T_p bw_{eff} = T_p bwdth/19.6 - 1.8. \quad [17]$$

Repetitive estimates of m_{RF} and c_{RF} varied a little at each value of ι_{bw} so the maximum values were accepted to eliminate uncertainty caused by second order oscillations in the data. A plot similar to Fig. 3 yielded ($r^2 = 0.9999$)

$$1/m_{RF}^2 = -7.916\iota_{bw} + 8.295 - 9.2 \times 10^{-4}/(1 - \iota_{bw}). \quad [18]$$

The dependence of c_{RF} on ι_{bw} for tanh/tan was also similar to that of c_{RF} on ι_o for the sech/tanh pulse, although it was found that the simpler equation,

$$c_{RF} = 0.13(1 - \iota_{bw})^{-0.5}, \quad [19]$$

fitted the data a little better ($r^2 = 0.999$) than the form of Eq. [10].

Equations [16]–[19] were checked for accuracy in a similar manner to the sech/tanh pulse. A total of 110 checks were made over the ranges $\iota_{bw} = 0.8$–0.99, $T_p = 0.05$–20 ms and $bw_{eff} =$ 1–400 kHz, yielding the ranges $T_p bw_{eff} = 4$–400 and $RF_{max} =$ 0.3–120 kHz. The error in predicting effective bandwidths was

an average of $+0.34 \pm 0.43\%$. The largest negative errors of -0.7% occurred for $T_p bw_{eff}$ values between 4 and 10 units and eliminating these the average is $+0.39 \pm 0.36\%$.

COMPARISON OF SECH/TANH AND TANH/TAN INVERSION PULSES

Although these two pulses differ markedly in many respects, the final master calibration equations have a similar form. Indeed, the similarity would be even closer if the numerical analysis of the sech/tanh pulse was repeated using the "variable *bwdth*" method since this would determine the optimum combination of $\Delta\iota$ and ι_o for fixed ι_{bw}, and thus be equivalent to substituting $\Delta\iota \approx 0.005$ and $\iota_o \approx \iota_{bw} + 0.005$ in Eqs. [9]–[11] and [13].

The availability of master equations for both pulses enables a direct comparison as in Fig. 9 for equivalent parameters. For the same RF_{max} and effective bandwidth the comparison shows that as expected (*4*) the pulse length of a tanh/tan pulse is always less than the equivalent sech/tanh pulse. The advantage is a factor of 2.4 for 20-kHz pulses reducing to 1.8 for 100-kHz effective bandwidths. However, this advantage is of value only if there is insufficient time in a pulse sequence for a sech/tanh pulse. For example, it has been noted above that a 1-ms sech/tanh pulse can be used without difficulty in a 3-ms J modulation delay, which could be the $(2J)^{-1}$ time for $^{13}C^{1}H$ coupling. From Fig. 9, effective bandwidths of 100 kHz can be readily achieved with 1-ms sech/tanh pulses using normal RF amplitudes available for ^{13}C irradiation.

Another marginal advantage arises from the finding that there is very little variation in scalar coupling modulation across the effective bandwidth for a tanh/tan pulse. Calculation of the average reduced coupling constant during the pulse is accomplished by substituting the expression

$$\tan\alpha = [\tan(0.968\pi T/2) + s]/[20v \tanh(10T)] \qquad [20]$$

into Eqs. [22] or [24] of Ref. (*5*) with Eq. [25] of (*5*) being replaced by

$$x = [\tan^{-1}(-s)]/(0.968\pi/2). \qquad [21]$$

This yields a very strong dependence of J_r/J_o on v, but this is insignificant in applications since tanh/tan operates at much lower values of v and offset s than equivalent sech/tanh pulses. For example, from Fig. 9a, a 1-ms sech/tanh pulse providing an effective bandwidth of 50 kHz requires $RF_{max} = 12$ kHz and from Eq. [11] the *bwdth* parameter must be set to 57 kHz so that $v = 2RF_{max}/bwdth = 0.42$. From Ref. (*5*), $J_r/J_o = 0.93$ at $s = 0$ decreasing to 0.8 at the edge of the effective bandwidth. From Fig. 9b, an equivalent 50-kHz tanh/tan pulse operating at a 12-kHz RF amplitude will have $T_p = 0.51$ ms and from Eq. [18], $bwdth = 1050$, so that v is only 0.02 units yielding $J_r/J_o = 0.81$ at $s = 0$ decreasing only slightly across the effective bandwidth

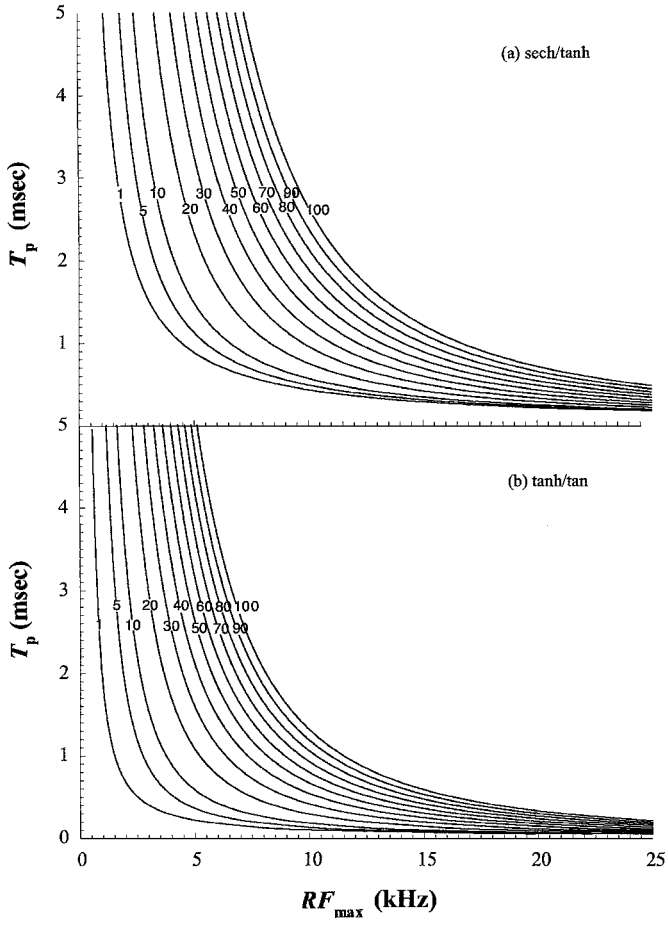

FIG. 9. Plots of T_p versus RF_{max} at various effective bandwidths ranging from 1 to 100 kHz for (a) the sech/tanh pulse at $\iota_o = 0.985$ and $\iota_{bw} = 0.980$ and (b) the tanh/tan pulse with bw_{eff} also measured at $\iota_{bw} = 0.980$. The comparison shows that for the same effective bandwidth in the range of 20 to 100 kHz and the same RF peak amplitude, the pulse length of a tanh/tan pulse is about half that of an equivalent sech/tanh pulse.

to 0.80 at the edge of bw_{eff} where $s = 0.05$. Thus the adjustment factor $(1 - J_r/J_o)$ arising from these complex calculations is adequately modelled for the tanh/tan pulse by a single polynomial for $v = 0$ to 0.1 at $s = 0$ by

$$(1 - J_r/J_o) = -0.0031 + 9.4653v - 42.817v^2. \qquad [22]$$

However, these modest advantages for the tanh/tan pulse come at a price: The total power delivered by a tanh/tan pulse, and thus the total contribution to sample heating, is considerably more than that of an equivalent sech/tanh pulse because the tanh function delivers close to constant RF amplitude throughout almost all of the pulse. Indeed, average RF power for the tanh function is given by

$$RF_{max}^2 \left(\int_0^{10} \tanh^2 x \, dx \right) \Big/ 10 = RF_{max}^2/1.11, \qquad [23]$$

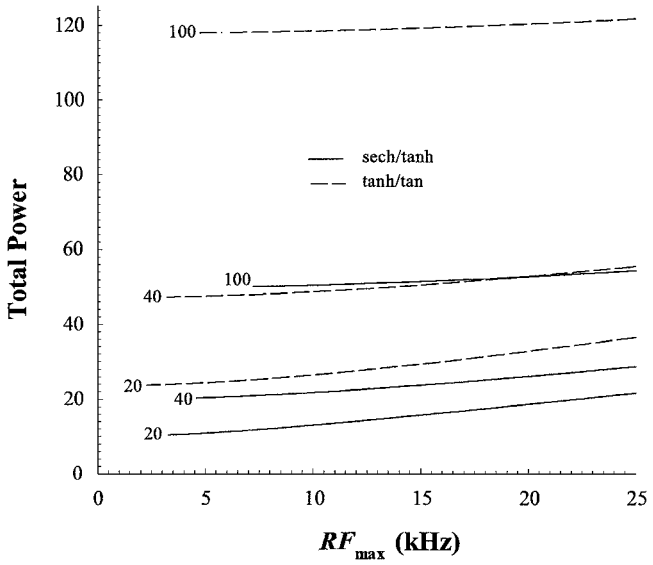

FIG. 10. Plots of total power delivered versus RF_{max} at $bw_{eff} = 20, 40$, and 100 kHz for the sech/tanh pulse at $\iota_o = 0.985$ and $\iota_{bw} = 0.980$ and the tanh/tan pulse with bw_{eff} also measured at $\iota_{bw} = 0.980$. T_p was in the range of 0.5 to 5 ms. The comparison shows that for the same effective bandwidth and the same RF peak amplitude, the power delivered by a tanh/tan pulse is about twice that of an equivalent sech/tanh pulse.

whereas for the sech amplitude function it is

$$RF_{max}^2\left(\int_0^{5.3} \text{sech}^2 x \; dx\right)\Big/ 5.3 = RF_{max}^2/5.3. \qquad [24]$$

To compare equivalent pulses having the same RF_{max}, and thus shorter pulse lengths for tanh/tan, total pulse power (= [average power]T_p) is plotted against RF_{max} in Fig. 10 for a range of effective bandwidths. For a 20-kHz effective bandwidth, the tanh/tan pulse delivers about twice the total power of an equivalent sech/tanh pulse and this factor increases to about 2.5 for 50–100-kHz bandwidth pulses.

PARTIAL ADIABATICITY

Partially Adiabatic sech/tanh and tanh/tan Pulses

The question of when an adiabatic pulse fails to be adiabatic goes beyond semantics and is a serious problem of definition. For example, Rosenfeld and Zur (*17*) devoted an entire paper to this problem as it concerns the sech/tanh pulse. Like many authors we have previously allowed the border between adiabatic and nonadiabatic to remain ambiguous and simply stated the qualitative definition that $|d\alpha/dt|/B_e$ should be small.

For sech/tanh, adiabaticity is obviously violated for $T_p bwdth$ values below about 10 units since the percentage inversion at zero offset oscillates markedly between 100% and lower values as RF_{max} is increased, and we have noted above that between 13 and 20 units sech/tanh departs by up to 4% from the linear master equations. Tanh/tan produces similar behavior at low values of $T_p bw_{eff}$. Thus, a reasonable quantitative definition of adiabaticity is the degree to which the pulse fits a straight line plot of $(RF_{max}T_p)^2$ versus $T_p bwdth$ or $T_p bw_{eff}$. We will call this "linear adiabaticity." Sech/tanh is "linearly adiabatic" to better than 5% for $T_p bwdth > 11$ and tanh/tan passes the same test for $T_p bw_{eff} > 3$.

Below these limiting values there is a complex transition region between "partial" and nonadiabaticity. In this nonlinear region both pulses provide effective bandwidths that are larger than those calculated by the linear master equations and so gain efficiency over the linear region. It is not possible to obtain universal equations for this complex region and instead some useful individual results are provided in Figs. 11–13. In Fig. 11 for $0.4 < T_p bw_{eff} < 1.4$, the tanh/tan pulse shows markedly greater

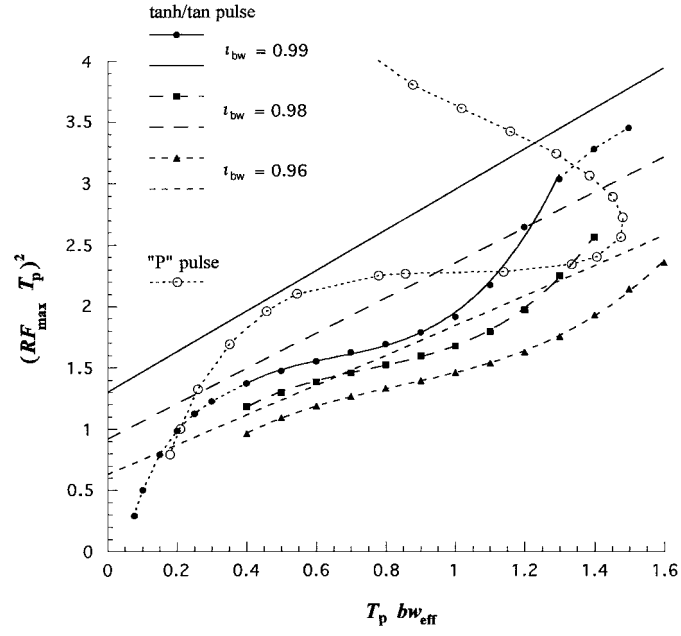

FIG. 11. Plots of optimal $(RF_{max}T_p)^2$ versus low values of $T_p bw_{eff}$ for the tanh/tan pulse at $\iota_{bw} = 0.99$, 0.98, and 0.96. At each value of ι_{bw}, the nonlinear behavior in this partially adiabatic region is contrasted with the linear calibrations that are accurate for $T_p bw_{eff} > 3$. The full extent of the curve is shown for $\iota_{bw} = 0.99$ terminating at coordinates (0.076, 0.29) that correspond to a zero frequency sweep and a completely nonadiabatic pulse. Each data point was obtained using the variable *bwdth* method by minimizing RF_{max} at constant T_p for a chosen value of bw_{eff}. To enable practical implementations of the efficient region, $0.4 < T_p bw_{eff} < 1.4$, the three curves are, respectively, modelled by the polynomials $0.041 + 5.93x - 8.20x^2 + 4.17x^3$; $0.001 + 4.77x - 5.58x^2 + 2.49x^3$; and $0.068 + 3.31x - 3.16x^2 + 1.25x^3$ (the necessary value of *bwdth* for a chosen bw_{eff} can be obtained from Fig. 12). An equivalent optimal plot for the P pulse of Ref. (*19*) was also obtained at $\iota_{bw} = 0.96$ by the "variable *bwdth*" method by maximizing bw_{eff} at constant T_p for a chosen value of RF_{max}. The P pulse curve terminates at (0.18, 0.79) corresponding to $bwdth = 0$. Variable *bwdth* was achieved by multiplying the phase table provided for the P pulse in (*19*) by a number between 0 and 10 since this is equivalent to varying the *bwdth* frequency-sweep parameter as exemplified by Eqs. [2] and [4] for sech/tanh and tanh/tan. The P pulse never obtains a lower value of $(RF_{max}T_p)^2$ than the tanh/tan pulse at $\iota_{bw} = 0.96$.

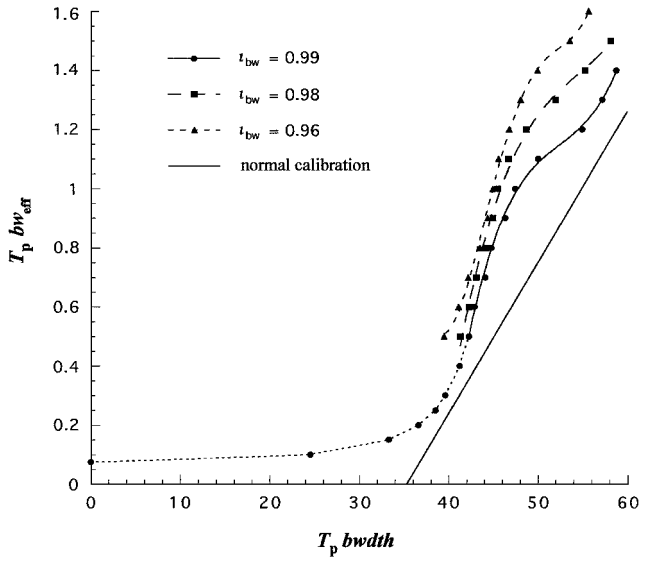

FIG. 12. Plots of the $T_p bw_{eff}$ versus $T_p bwdth$ values used to produce the optimal curves for the tanh/tan pulse under partially adiabatic conditions in Fig. 11. The calibration for linear adiabaticity, effective above $T_p bw_{eff} = 3$, is shown for comparison. The fitted polynomials for $\iota_{bw} = 0.99$, 0.98, and 0.96 are, respectively, $-56.1 + 3.23x - 0.0611x^2 + 3.88 \times 10^{-4}x^3$; $-39.5 + 2.19x - 0.0397x^2 + 2.42 \times 10^{-4}x^3$; and $397.2 - 33.84x + 1.071x^2 - 0.0149x^3 + 7.73 \times 10^{-5}x^4$. Additional data points are provided for $\iota_{bw} = 0.99$ illustrating the dependence of bw_{eff} versus $bwdth$ as the latter is reduced to zero and the pulse becomes completely nonadiabatic at the termination coordinates (0, 0.076).

efficiency than the linear calibrations. For example, an 80-μs pulse yields a minimum of 99.5% inversion efficiency across 10 kHz yet this is readily achievable with $RF_{max} = 16$ kHz. An equivalent rectangular pulse requires $RF_{max} = 70$ kHz. Garwood (*18*) has recently highlighted the efficiency of a tanh/tan pulse under conditions identical to those in Fig. 11 at $T_p bw_{eff} = 0.3$ ($T_p bwdth = 40$).

A detailed analysis of any adiabatic pulse at high RF amplitude shows that the spin magnetization revolves rapidly around the effective field B_e as the latter rotates from the z to the $-z$ axis. The number of revolutions decreases with lower RF_{max} and $bwdth$ and the center of the region, $0.4 < T_p bw_{eff} < 1.4$, for tanh/tan corresponds approximately to just one complete revolution. A further reduction of RF_{max} and $bwdth$ is shown in Figs. 11 and 12 for $\iota_{bw} = 0.99$ until at $bwdth = 0$ there is no frequency sweep and the curve terminates in both figures. At this end point, tanh/tan has become a simple amplitude-modulated tanh-only pulse, like a rectangular pulse, characterized by a one-half spin revolution at right angles to B_e with B_e stationary along the x axis. All amplitude modulated pulses (no frequency or phase shift) are completely nonadiabatic and correspond to a single coordinate in a plot of $(RF_{max} T_p)^2$ versus $T_p bw_{eff}$. For example, for $\iota_{bw} = 0.99$, the rectangular pulse is at (0.071, 0.25), a one-lobe sinc is at (1.01, 0.72), and the Gaussian pulse has coordinates of (1.32, 1.49).

Conversely, all frequency swept pulses must be partially adiabatic since a component of the spin magnetization, originally aligned with B_e, will rotate with B_e. A widely accepted property of adiabaticity is that spin manipulations are insensitive to increases in RF amplitude. For tanh/tan at $T_p bw_{eff} = 0.9$ and $\iota_{bw} = 0.96$ the percentage inversion oscillates as the RF amplitude is increased. This is expected for partial adiabaticity, but an increase of more than 3.2 times in RF_{max} above the optimal value in Fig. 11 is required before the percentage inversion falls below 95%. Partially adiabatic pulses are thus obviously useful in high resolution NMR when compensation for variable RF is required.

The partially adiabatic region for sech/tanh is illustrated in Fig. 13, with the RF y-axis dependence changed to average power times T_p^2 to enable a comparison with other pulses. Figure 13 illustrates the expected divergence of sech/tanh from the linear calibration to more efficient conditions at low $T_p bw_{eff}$,

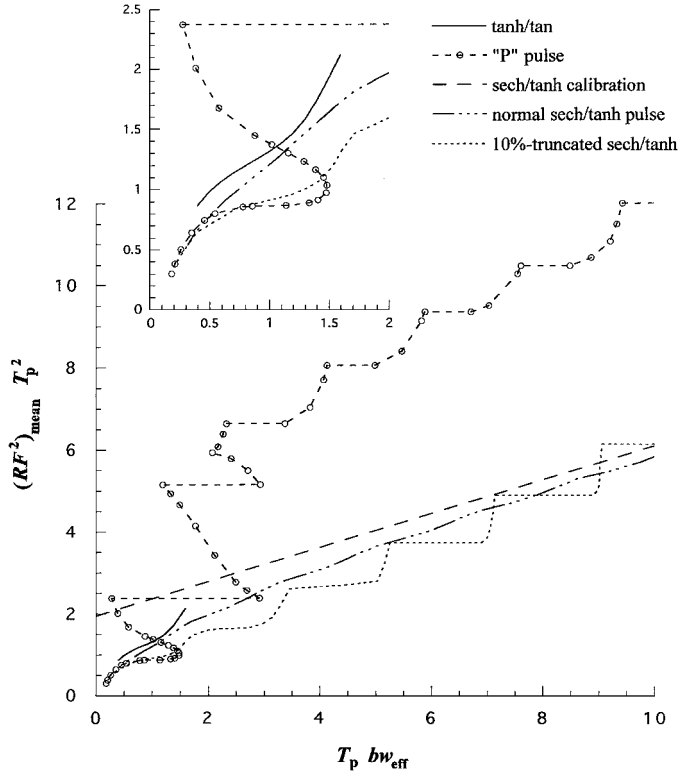

FIG. 13. Plots of optimal $(RF^2)_{mean}\ T_p^2$ versus low values of $T_p bw_{eff}$ at $\iota_{bw} = 0.96$ for the tanh/tan pulse; the P pulse of Ref. (*19*); the sech/tanh pulse truncated normally at 1%; and the sech/tanh pulse truncated at 10%. The data were obtained as described in the caption to Fig. 11 but the y axis has been changed to average RF^2, and thus average power, times T_p^2 by dividing $(RF_{max})^2$ by 1.11, 2.63, 5.3, and 3.0, respectively, for the four different pulses (e.g., see Eqs. [23] and [24]). The calibration for linearly adiabatic sech/tanh is also plotted for comparison. The complex area at lowest $T_p bw_{eff}$ is expanded in the inset illustrating a marginal average power advantage for the P pulse over 10%-truncated sech/tanh for a restricted region of $T_p bw_{eff}$. The discontinuous horizontal sections evident for these two pulses are caused by wobbles on the inversion profiles resulting from the large truncation factors.

but sech/tanh is only slightly more efficient than the best portion of the tanh/tan curve reproduced from Fig. 11.

As shown in Fig. 13, and also found for sech/tanh decoupling (STUD (*10*)), greater power efficiency can be obtained at low $T_p bw_{eff}$ by increasing the truncation level of the pulse from a standard 1% ($\beta = 5.3$) to 10% ($\beta = 3.0$). This large truncation induces wobbles across the inversion profile that exceed $1 - \iota_{bw}$ and successively add and subtract from bw_{eff} causing the stepped nature of the resulting calibration "curve." Interestingly, each step from right to left in Fig. 13 corresponds to a reduction of one in the number of spin revolutions about B_e, a direct indication of this phenomenon described above for tanh/tan. The curve between 0.5 and 2 units is reproduced in the inset to Fig. 13 and shows a considerable advantage for 10%-truncated sech/tanh over the best tanh/tan result in terms of average power. This greater efficiency comes at a price in terms of increased sensitivity to increasing the RF amplitude. For example, at $T_p bw_{eff} = 1.4$ and $\iota_{bw} = 0.96$, normal sech/tanh inversion never falls below 93% for any increased value of RF_{max}, whereas a 2.5 times increase in RF for the 10%-truncated pulse yields 90% inversion at the edges of bw_{eff}. This is nevertheless a good result for practical applications.

The Partially Adiabatic "P" Pulse

In addition to distinguishing partial and linear adiabaticity, plots of $(RF_{max} T_p)^2$ or (average power)T_p^2 versus $T_p bw_{eff}$ provide a means of directly comparing the properties of different types of RF pulses.

The recent "P" pulse of Barker *et al*. (*19*) was claimed to be "numerically optimized nonadiabatic frequency- and amplitude-modulated," but being frequency swept it must be partially adiabatic. For example, the amplitude and frequency waveforms of the P pulse are similar to those of 10%-truncated sech/tanh. The P pulse was designed to be optimum for $T_p bw_{eff} \approx 1$ and this, and its partial adiabaticity, is confirmed in the comparative simulations in Figs. 11 and 13.

Figure 13 demonstrates that at high values of $T_p bw_{eff}$ the P pulse enters a linearly adiabatic region modified to a stepped dependence like that of the 10%-truncated sech/tanh pulse. The steps are larger for the P pulse since it is truncated at 22% of RF_{max}. The numerical optimization procedure has produced a "sweet spot" in the $0.5 < T_p bw_{eff} < 1.5$ region and this is more clearly illustrated in the inset to Fig. 13. In comparison to 10%-truncated sech/tanh, the P pulse provides a maximum 15% advantage in average power for $1 < T_p bw_{eff} < 1.5$, but is much worse everywhere else. The P pulse is also five times more sensitive to increases in RF amplitude than 10%-truncated sech/tanh at $T_p bw_{eff} = 1.4$ and $\iota_{bw} = 0.96$, although it retains some residual adiabaticity by being 1.7 times less sensitive than a rectangular pulse. Furthermore, an increase in the sech/tanh truncation above 10% would further reduce any P pulse advantage. The P pulse curve for $\iota_{bw} = 0.96$ is also plotted in Fig. 11 proving that tanh/tan at the same RF_{max} always requires a smaller pulse length. The insensitivity of tanh/tan to RF inhomogeneity is also vastly superior. Thus the numerical optimization of the P pulse is a fair attempt at eliminating the benefits of adiabaticity, but has not achieved much in terms of reducing average power or pulse length in comparison to the well known analytic adiabatic pulses.

The 15% power advantage of the P pulse over 10%-truncated sech/tanh may be a worthwhile advantage for repetitive use in spin decoupling. This is the application described by Barker *et al*. (*19*) and for the first time they have demonstrated a power advantage over composite pulse decoupling at a narrow bandwidth. In relation to previous work (e.g., (*9, 10*)) this was unexpected because adiabatic decoupling dominates for large bandwidths but falls short of the efficiency of composite pulse decoupling at small bandwidths. The results in Fig. 13 now explain this new finding—frequency swept pulses gain in efficiency in the partially adiabatic region compared to the equations governing linear adiabaticity. For example, at $T_p bw_{eff} = 1$, partially adiabatic sech/tanh is twice as efficient as the level given by the linear calibration.

Nevertheless, if previous developments are transferred to partially adiabatic decoupling, the P pulse may not show any worthwhile gains over analytic waveforms such as sech/tanh. For STUD+ decoupling (*10*) it was found that use of a sophisticated phase cycle permitted a reduction in RF amplitude so that each inversion need only be 85% complete on average. Barker *et al*. (*19*) employed a simple 4-phase cycle and numerically optimized the P pulse to achieve high inversion efficiency as at $\iota_{bw} \approx 0.96$ in Fig. 13. But at $\iota_{bw} \approx 0.7$ (85% inversion) the P pulse is 40% less efficient in terms of power than 10%-truncated sech/tanh. We suggest that a detailed analysis of partially adiabatic decoupling should begin with the sech/tanh pulse and numerical optimization should be employed to improve on that baseline result, but such a major study is beyond the scope of this article.

Partially Adiabatic BIPs

The common authors of Refs. (*19, 20*) appear to concur with our observation that the P pulse is partially adiabatic since in (*20*) they have developed a series of broadband inversion pulses (BIPs) that are explicitly described as partially adiabatic. Our respective notions of partial adiabaticity now seem similar, although we have quantified the meaning of "partial adiabaticity" relative to "linear adiabaticity." BIPs were designed with their adiabaticities reduced by numerical optimization to reduce their compensation for RF inhomogeneity and increase their RF power efficiency. Thus, similar to the P pulse, each BIP is optimized for a single coordinate on a plot of $(RF_{max} T_p)^2$ versus $T_p bw_{eff}$. BIPs use constant amplitude and numerically optimized frequency sweeps and provide impressive results in terms of low values of RF_{max} and T_p for a required bw_{eff}. The broadest bandwidth example is described as "dwarfing" analytic adiabatic pulses, including the tanh/tan pulse. The difficulty with this

claim is that although the BIPs were numerically optimized, no consideration was given to optimizing the analytic waveforms of the adiabatic pulses (not even their truncation factors) to increase their RF power efficiency. Furthermore, the BIPs were compared with adiabatic pulses utilizing non-optimal combinations of $RF_{\max}$, T_p and *bwdth*. For example, the "dwarfing" comment referred to tanh/tan at $R = T_p\ bwdth = 110$ whereas the optimal value is 412.

To assist proper comparisons, the notation in Ref. (*20*), BIP-*dd-xx-yy*, translates as

$$T_p bw_{\text{eff}} = 2 * (xx/100) * (dd/360); \quad [25]$$

$$RF_{\max} T_p = (dd/360) * (1 - yy/100). \quad [26]$$

The correction factor, $(1 - yy/100)$, ensures that the lowest RF amplitude for a BIP over its optimized range is used for comparison with the optimal minimum value obtained from the tanh/tan master Eqs. [16]–[19]. In the following list, $\iota_{bw} = 0.96$ so that the percentage inversion of tanh/tan matches that of each BIP. Generally this allowed for tanh/tan to perform slightly worse at the lowest $RF_{\max}$ for the BIP and slightly better at its highest $RF_{\max}$ (and of course ever better as RF is increased beyond that value). For the 12 BIPs in the order presented in Table 1 of (*20*) the following list takes the format, *dd-xx-yy* ($T_p bw_{\text{eff}}$, $RF_{\max} T_p$, **% comparison**): *360-30-5* (0.6, 1, **−5%**); *360-20-10* (0.4, 1, **−17%**); *360-5-25* (0.1, 1, **+50%**); *540-50-15* (1.87, 1.5, **−18%**); *720-100-10* (4, 2, **−23%**); *720-50-20* (2, 2, **−11%**); *720-25-40* (0.5, 2, **+14%**); *720-75-15* (3, 2, **−18%**); *810-90-15* (4.05, 2.25, **−19%**); *900-100-15* (6.25, 2.5, **−26%**); *900-120-20* (6, 2.5, **−27%**); *1382-250-15* (19.2, 3.84, **−23%**). (The number *50* for the fourth pulse has been changed from *75* in (*20*) as our simulations indicated a typing error.) The percent comparison value in each case (in boldface) is the percentage by which the necessary $RF_{\max}$ for the BIP exceeds (positive) or is less than (negative) that required for tanh/tan. The best results for the BIPs are for large bandwidths compared to $RF_{\max}$ and reduced compensation for RF inhomogeneity. Discarding the remainder plus those at very low $T_p bw_{\text{eff}}$, and thus the poor results, yields modest advantages of 11–27% for BIPs over normal tanh/tan.

However, these apparent 11–27% gains of BIPs over tanh/tan are largely illusory because no attempt has been made to optimize the standard tanh/tan analytic waveforms to specifically reduce the required $RF_{\max}$. Historically (*3, 4*), the tanh/tan pulse was introduced to eliminate the large (≈5%) wobbles on the inversion profile produced by the constant/tan pulse (*8*). These wobbles, induced by the discontinuous rectangular amplitude function, are eliminated by the smooth tanh sweep at a cost of increasing $RF_{\max}$ by 7% to provide the same average RF amplitude. In unpublished work (M. Garwood, personal communication (2001)) the originators of tanh/tan realized during the preparation of Ref. (*3*) that the pulse could be made more efficient in terms of a lower $RF_{\max}$ or T_p by changing the truncation of the tanh and tan functions, but the modest gains were counterbalanced by a loss in compensation for RF inhomogeneity. The values chosen, tanh(10) and $\tan\kappa = 20$, preserved the tolerance to a factor of 10 increase in RF, suitable for *in vivo* NMR, but still allowed for short pulses applicable to high resolution NMR—a truly universal RF pulse! In some nonexhaustive simulations we have found that the BIP efficiencies can be approached by tanh/tan employing large reductions of the tan truncation from the value of 20. For example, BIP-*1382-250-15*, can be closely matched by a tanh/tan pulse with $\tan\kappa = 1.34$, $bw_{\text{eff}} = 100$ kHz, $bwdth = 241$ kHz, $T_p = 192\ \mu$s, and $RF_{\max} = 21.44$ kHz, compared to $RF_{\max} = 20$ kHz for the BIP. Both pulses exceed $\iota_{bw} = 0.895$ (94.8% inversion) at $0.85RF_{\max}$, the tanh/tan pulse is slightly worse at $1.0RF_{\max}$, slightly better at $1.15RF_{\max}$ and then increasingly superior as the RF amplitude is further increased. The BIP advantage in terms of $RF_{\max}$ is just 7%, the same proportional difference required to maintain the same average RF when changing from constant amplitude to the tanh function. This translates to a 14% reduction in T_p at the same $RF_{\max}$ and bw_{eff}, or equivalently the BIP "dwarfs" tanh/tan to the extent of 14% in bandwidth at the same T_p and $RF_{\max}$. Strikingly, although the truncation impairs the ability of tanh/tan to compensate for RF inhomogeneity, it still compensates for a gargantuan 4 times increase in $RF_{\max}$ compared to just ±15% for the BIP.

Another drawback is that each BIP is optimized for a single coordinate on a plot of $(RF_{\max} T_p)^2$ versus $T_p bw_{\text{eff}}$. The values for these coordinates can be obtained from the above list. If the value of $T_p bw_{\text{eff}}$ is varied by 50% the advantage of having a lower $RF_{\max}$ is lost and the BIP no longer inverts as well as an equivalent tanh/tan pulse. To be competitive, a large online library of unique BIPs is required at say 10% increments in $T_p bw_{\text{eff}}$ to cover the entire range implementable with a simple macro for the analytic tanh/tan pulse.

A possible explanation for the failure of the BIP strategy expressed in Ref. (*20*) can be found by examining BIP-*1382-250-15* relative to our notions of partial and linear adiabaticity. The waveforms for this BIP are similar to a truncated constant/tan ($\tan x \approx 4$) pulse. Thus, the above discussion of the development of tanh/tan from constant/tan is doubly apt. To easily analyze either constant/tan or this BIP over a large range of conditions it is necessary to choose a low ι_{bw} to avoid the ≈5% amplitude truncation wobbles and thus avoid the type of discontinuities exemplified by the P pulse in Fig. 13. Choosing $\iota_{bw} = 0.8$, the BIP yields a linear plot of $(RF_{\max} T_p)^2$ versus $T_p bw_{\text{eff}}$ with a scatter of data points that is the residual product of the discontinuities. This plot was made using the "variable *bwdth*" method and multiplying the phase modulation provided in (*20*) by a number N to vary *bwdth*. The plot is linear over any range that exceeds the period of the discontinuities evident at higher ι_{bw}. The BIP numerical optimization produces a large nonlinear detour to lower and more efficient values of $(RF_{\max} T_p)^2$ at $N \approx 1$ but this is only evident at these higher ι_{bw} values. Furthermore, the ≈5% wobbles are suppressed at N values close to unity. Thus, the BIPs are basically linear adiabatic pulses. The numerical optimizations

are almost entirely devoted to trading adiabaticity (and the compensation for RF variance) as a means to suppress the truncation wobbles that were regressively reintroduced via the discontinuous rectangular amplitude function. Little is achieved in the overall reduction of $RF_{\max}$.

CONCLUSIONS

This analysis of adiabatic sech/tanh and tanh/tan pulses shows that their inversion properties are constant over a wide range of conditions provided that

$$(RF_{\max}T_p)^2 = m_1 T_p bwdth + c_1, \quad [27]$$

$$(RF_{\max}T_p)^2 = m_2 T_p bw_{\text{eff}} + c_2, \quad [28]$$

since $T_p bwdth$ and $T_p bw_{\text{eff}}$ are also linearly related as

$$T_p bwdth = m_3 T_p bw_{\text{eff}} + c_3. \quad [29]$$

These relationships break down at low values of T_p *bwdth* where the pulses become partially adiabatic.

The intercept c_1 in Eq. [27] is quite small for both pulses and if this is set to zero the equation becomes $RF^2_{\max}T_p/bwdth = m_1$. It was noted from Eq. [5] that this quantity is related to adiabaticity and in Ref. (*21*) the reciprocal of Eq. [5] was defined as the adiabaticity factor Q. For zero offset, $Q = (2\pi/5.3)RF^2_{\max}T_p/bwdth$ for the sech/tanh pulse at the middle of the adiabatic sweep, so the dominant relationship in Eq. [27] is obviously the adiabaticity of the pulse. Nevertheless, there appears to be no way to prove Eqs. [27]–[29] algebraically, hence our numerical approach.

A proportionality between average power ($\propto RF^2_{\max}$) or total pulse power ($\propto RF^2_{\max}T_p$) and bandwidth (*bwdth* or bw_{eff}) at constant pulse length T_p has been variously suggested before (e.g., (*9, 10, 22*)). Master equations [27] or [28] take this one step further. Appropriate multiplication by T_p yields dimensionless quantities that are proportional under all conditions if $c_1 = c_2 = 0$. Thus, while it may not be surprising that these constants, c_1 and c_2, are small, their origin is not obvious and it is serendipitous that they are independent of $RF_{\max}$, T_p, and *bwdth*.

The different behavior of the two pulses, exemplified by their profiles drawn in Fig. 1, induced a different course of analysis for the two cases. These can be reconciled by setting $\Delta\iota = 0.005$ and $\iota_o = \iota_{bw} + 0.005$ in Eqs. [9]–[11] and [13] for the sech/tanh pulse. The result is that the slopes m_n and intercepts c_n of Eqs. [27]–[29] depend only on the minimum selected extent of inversion, ι_{bw}, across the effective bandwidth, bw_{eff}. The differences between the two types of pulse are then entirely manifested in the different numerical constants in the equations of $m_n = f(\iota_{bw})$ and $c_n = f(\iota_{bw})$. Since the two types of pulse behave quite differently, yet provide the same form of master equations [27]–[29], we confidently suggest that all adiabatic pulses will behave in this way. While some residual doubt may remain concerning this conclusion, it certainly applies to the infinite number of pulses comprising the family of "constant adiabaticity" pulses (*22, 23*), which includes the sech/tanh pulse. Overall the analysis determined the optimum conditions for application for the two types of pulse in terms of three independent and two dependent variables.

Two concepts have been defined, "linear adiabaticity" applicable to the behavior of adiabatic pulses under conditions where linear master equations of the form of Eqs. [27]–[29] apply, and "partial adiabaticity," which we have used to describe the behavior at lower values of $T_p bwdth$ or $T_p bw_{\text{eff}}$. In these terms a pulse can be said to be adiabatic when it complies with these equations to some defined level of accuracy, hence providing an exact measure of adiabaticity.

During this study the "variable *bwdth*" method was devised to produce plots of $(RF_{\max}T_p)^2$ versus $T_p bw_{\text{eff}}$ for optimal conditions. Our experience suggests that this is a general method for any RF inversion pulse. Any adiabatic pulse will produce a linear plot above some limiting value of the x or y coordinate. Any partially adiabatic pulse, which includes all frequency or phase modulated pulses that are not linearly adiabatic, will produce a more complex curve. Pulses that are only amplitude modulated are characterized by a single coordinate in the 2D plot. Such plots permit the direct comparison of the relative performance of any RF inversion pulses and it is hoped that new pulses will be compared with existing pulses in this way at the time of their invention. For adiabatic pulses there is also the facile alternative of quantitatively comparing the results of their respective linear master equations.

It appears that plots of $(RF_{\max}T_p)^2$ versus $T_p bw_{\text{eff}}$ for any linearly adiabatic pulse will have a positive y intercept. Thus, plots in the partially adiabatic region must curve downwards from the linear region to terminate close to the origin. Accordingly, partially adiabatic pulses must always be more efficient in terms of pulse length and RF amplitude than linearly adiabatic pulses. This advantage is accompanied by the reintroduction of tip-angle dependence on increasing RF amplitude in contrast to the insensitivity of adiabatic pulses in the linear region. However, this dependence is modest for the tanh/tan and sech/tanh pulses in the partially adiabatic region except close to the termination point.

These general methods of assessing the properties of linear and partial adiabatic pulses were used to examine the partially adiabatic P pulse of Barker *et al.* (*19*) and BIP pulses of Smith *et al.* (*20*). These numerically optimized pulses demonstrate modest gains of up to about 10% in either total power or maximum RF amplitude over comparable applications of the analytic sech/tanh or tanh/tan pulses with appropriate truncation factors. This modest improvement is accompanied by a large loss of adiabaticity and thus a large increase in sensitivity to RF inhomogeneity. Furthermore, each numerically optimized pulse is only useful for a single product of pulse length and effective bandwidth, like composite pulses but unlike normal adiabatic pulses.

By comparing BIPs to examples of the tanh/tan pulse with a highly truncated tan function, we concluded that the effort of numerical optimization, and the inevitable sad loss of adiabaticity, has been devoted largely to suppressing the deleterious effects of reintroducing a constant amplitude waveform, an outmoded concept (*3, 7, 8*), into the BIPs. If a general 20% reduction in RF_{max} relative to the standard tanh/tan pulse is seen to be of real value in high resolution NMR, then the two truncation factors inherit in the tanh/tan functions should be optimized. A detailed method for doing this has been presented in this paper, but tedious optimizations over two further parameters require a computerized approach, beyond the goals of the present study. However, the methods established here, primarily the optimization of $(RF_{max}T_p)^2$ versus $T_p bw_{eff}$ dependencies, are ripe for digital exploitation.

Optimization of the analytical forms of normal adiabatic pulses is a worthwhile goal since the master equations applicable to these linearly adiabatic pulses will always be valid for a wide range of effective bandwidths and pulse lengths, yet still compensate for large RF inhomogeneities. Numerical optimizations that sacrifice adiabaticity and are specific to particular combinations of pulse length and effective bandwidth are of less value even when proven to be more efficient than the original pulses. For example, in relation to STUD+ decoupling (*10*) we noted that 5–10% gains could be made by numerical optimization (similar to the BIP gains over truncated tanh/tan). However, this work has not been published since these modest improvements are outweighed by the ease of implementing the analytic sech/tanh waveform over a wide range of conditions using a simple computer macro.

ACKNOWLEDGMENT

We thank Dr. Mike Garwood for reviewing the manuscript and providing details concerning the development of the tanh/tan pulse, helpful comments, and other constructive criticisms.

REFERENCES

1. P. C. M. van Zijl, T.-L. Hwang, M. O'Neil Johnson, and M. Garwood, Optimized excitation and automation for high resolution NMR using $B1$ insensitive rotation pulses, *J. Am. Chem. Soc.* **118,** 5510–5511 (1996).
2. M. S. Silver, R. I. Joseph, and D. I. Hoult, Selective spin inversion in nuclear magnetic resonance and coherent optics through an exact solution of the Bloch–Riccati equation, *Phys. Rev. A.* **31**(4), 2753–2755 (1985).
3. M. Garwood and Yong Ke, Symmetric pulses to induce arbitrary flip angles with compensation for RF inhomogeneity and resonance offsets, *J. Magn. Reson.* **94,** 511–525 (1991).
4. T.-L. Hwang, P. C. M. van Zijl, and M. Garwood, Fast broadband inversion by adiabatic pulses, *J. Magn. Reson.* **133,** 200–203 (1998).
5. M. R. Bendall, Heteronuclear J-coupling precession during spin-lock and adiabatic pulses: Use of adiabatic inversion pulses in high-resolution NMR, *J. Magn. Reson. A* **116,** 46–58 (1995).
6. M. R. Bendall and T. E. Skinner, Comparison and use of vector and quantum representations of J-coupled spin evolution in an IS spin system during irradiation of one spin, *J. Magn. Reson.* **143,** 329–351 (2000).
7. V. J. Basus, P. D. Ellis, H. D. W. Hill, and J. S. Waugh, Utilization of CHIRP frequency modulation with 180°-phase modulation for heteronuclear decoupling, *J. Magn. Reson.* **35,** 19–37 (1979).
8. C. J. Hardy, W. A. Edelstein, and D. Vatis, Efficient adiabatic fast passage for NMR population inversion in the presence of radiofrequency field inhomogeneity and frequency offsets, *J. Magn. Reson.* **66,** 470–482 (1986).
9. M. R. Bendall and T. E. Skinner, Calibration of STUD decoupling to achieve selected sideband amplitudes, *J. Magn. Reson. A* **120,** 77–87 (1996).
10. M. R. Bendall and T. E. Skinner, Calibration of STUD+ parameters to achieve optimally efficient broadband adiabatic decoupling in a single transient, *J. Magn. Reson.* **134,** 331–349 (1998).
11. K. Ugurbil, M. Garwood, and A. R. Rath, Optimization of modulation functions to improve insensitivity of adiabatic pulses to variations in $B1$ magnitude, *J. Magn. Reson.* **80,** 448–469 (1988).
12. D. Rosenfeld, S. L. Panfil, and Y. Zur, Optimization of adiabatic selective pulses, *J. Magn. Reson.* **126,** 221–228 (1997).
13. E. Lunati, P. Confrancescon, M. Villa, P. Marzola, and A. Sbarbati, Evolution strategy optimization for adiabatic pulses in MRI, *J. Magn. Reson.* **138,** 48–53 (1999).
14. Z. Starcuk, Z. Starcuk, V. Mlynarik, M. Roden, J. Horky, and E. Moser, Low-power water suppression by hyperbolic secant pulses with controlled offsets and delays, *J. Magn. Reson.* **152,** 168–178 (2001).
15. T. E. Skinner and M. R. Bendall, A vector model of adiabatic decoupling, *J. Magn. Reson.* **134,** 315–330 (1998).
16. H. Geen and R. Freeman, Band-selective radiofrequency pulses, *J. Magn. Reson.* **93,** 93–141 (1991); C. Roumestand, J. Mispelter, C. Austruy, and D. Canet, The use of band filtering in multidimensional NMR, *J. Magn. Reson. B* **109,** 153–163 (1995).
17. D. Rosenfeld and Y. Zur, Is the sech/tanh adiabatic pulse really adiabatic, *J. Magn. Reson.* **132,** 102–108 (1998).
18. M. Garwood, Using adiabatic rapid passage to minimize rf power requirements in NMR, *in* "Integrated Human Brain Science" (T. Nakada, Ed.), Chap. II.3, pp. 79–89, Elsevier, Amsterdam (2000).
19. P. B. Barker, X. Golay, D. Artemov, R. Ouwerkerk, M. A. Smith, and A. J. Shaka, Broadband proton decoupling for *in vivo* brain spectroscopy in humans, *Magn. Reson. Med.* **45,** 226–232 (2001).
20. M. A. Smith, H. Hu, and A. J. Shaka, Improved broadband inversion performance for NMR in liquids, *J. Magn. Reson.* **151,** 269–283 (2001), doi:10.1006/jmre.2001.2364.
21. J. Baum, R. Tycko, and A. Pines, Broadband and adiabatic inversion of a two-level system by phase-modulated pulses, *Phys. Rev. A.* **32,** 3455–3447 (1985).
22. A. Tannus and M. Garwood, Improved performance of frequency swept pulses using offset independent adiabaticity, *J. Magn. Reson. A* **120,** 133–137 (1996).
23. E. Kupce and R. Freeman, Optimized adiabatic pulses for wideband spin inversion, *J. Magn. Reson. A* **118,** 299–303 (1996).